Rational-Designed Hybrid Aerogels for Ultra-Flyweight Electrochemical Energy Storage

Mingxia Lu[a], Shanshan Liu[a], Jing Chen[a], Xia Zhang[a], Jingchao Zhang[b], Zhe Li[c] and Bo Hou[d,]*

[a] School of Chemistry and Chemical Engineering, Henan University of Technology, Zhengzhou 450001, P. R. China

[b] Department of Biostatistics and Bioinformatics, Emory University, Atlanta, GA, 30322, USA

[c] School of Engineering and Materials Science, Queen Mary University of London, Mile End Road, London E1 4NS, United Kingdom

[d] Department of Physics and Astronomy, Cardiff University, Cardiff CF24 3AA, Wales, United Kingdom

*Corresponding author. Email: HouB6@cardiff.ac.uk, Tel: +44 (0)29 22510756. (Bo Hou)

ABSTRACT:

Hybridising 2D materials into 3D aerogels have attracted considerable interest in ultralight electrochemical energy storage devices. However, to optimise the device structure for more efficient charge storage and transport, a better understanding of the ratio-dependent hybridisation process and interface charge transfer mechanisms are highly required. Here, we perform a comprehensive study to elucidate the fundamental process during the reduced graphene oxide (rGO) and carbon nanotube (CNT) hybridisation, which enabled the fabrication of a rational-designed rGO/CNT hybrid aerogel (GCA) with a record energy storage

performance beyond previously reported works. Based on spectroscopy and microscopy analysis, we found the hydrophilic and hydrophobic transition of GO which eliminates the surface-functionalised oxygen-containing moieties, is the origin of the π-π stacking hybridisation between rGO and CNTs. Moreover, we found the different amount of CNTs 'solder' in-between rGO sheets can offer GCA distinct mechanical elasticity, ion diffusion resistance and specific capacitance. As illustrated in the electrochemical impedance spectroscopy (EIS) and charge/discharge analysis, we found GCA 2-2 (rGO:CNT=2:2) display the best gravimetric capacitance of 117 $F \cdot g^{-1}$ at a discharge current density of 1 $A \cdot g^{-1}$, which help us to fabricate an ultra-flyweight supercapacitor with a large energy density of 3.53 $Wh \cdot kg^{-1}$ at a power density of 283.4 $W \cdot kg^{-1}$.

INTRODUCTION

Miniaturisation and integration are new challenges in modern electronic devices with an emerging focus on wearable electronics.[1] Due to close contact with the human body, wearable devices require low weight, biocompatibility, small size, and flexibility.[2-5] Flexible and lightweight energy storage devices are essential for powering new-generation wearable electronics.[6-8] The supercapacitor (SC) is one of the promising devices for these portable energy-storage applications as their energy densities are much higher than conventional capacitors and possess much better power delivery capabilities than batteries.[9-10] At present, carbon is primary electrode materials used in SCs due to their abundant sources and facile modification processes.[11] Among them, electrical double-layer capacitors (EDLCs) are most

common device configuration,[12-14] whereas pure nonreactive carbon materials store charges electrostatically.[15-17] Indeed, in porous carbon materials with sub-nanometre pores, the desolvation of the ions leads to surprisingly high capacitances.[10, 18]

Lowering the weight of carbon electrode materials for ultralight as well as increase porosity, and specific surface area are new challenges in carbon-based supercapacitors.[19-21] Generally, three-dimensional (3D) aerogel, such as Graphene aerogel (GA), can be fabricated by using two-dimensional graphene oxide (GO) which can generate a 50% higher specific capacitance (152 $F \cdot g^{-1}$) than normal GO agglomerate particles-based SCs together with extremely lightweight.[22] GO is oxidised graphite flakes with excellent hydrophilicity associated with abundant oxygen-containing functional groups attaching to the edges and planes.[10, 23-24] However, due to the randomly distributed pore wall structure, GA shows low electrical conductivity, high brittleness, and can be easily collapsed under pressure.[25-26] Therefore, preparing a 3D framework GA with both high electrical conductivity and super-elasticity for high-performance supercapacitors is high demand.

Conductive and robust materials have been tried to blend into GA for enhancing the electrical conductivity, elasticity and specific capacitance.[14, 25, 27] However, GO has strong hydrophilic surface properties which give rise to difficulties for hybridising with other carbon materials such as hydrophobic carbon nanotubes.[10] Recently, the graphene/carbon nanotube hybrid aerogels (GCA) have shown some promise in improving specific capacitance (252 $F \cdot g^{-1}$ at 0.5

$A \cdot g^{-1}$) and stability associated with their high electrical conductivity, excellent mechanical strength, and proprietary hollow structures.[27] However, GO, and CNTs are difficult to be miscible with each other because of the low solubility of CNTs in water. Therefore, polymers, ionic liquid or cellulose nanofibrils are usually employed for dispersing CNT or GO, which not only makes the fabrication process complicates but also adds additional weight to the electrodes.[10, 27-29] Furthermore, to optimise the device structure to allow for more efficient charge storage and transport, a better understanding of the ratio-dependent hybridisation process as well as interface charge transfer mechanisms that take place in these proprietary hollow structures are highly required.

In this work, we fabricated the super-elastic graphene/carbon nanotube aerogels (GCA) by stepwise hydrothermal and freeze-drying process. The effect of CNT content on the structure, electrical conductivity and specific capacity of GCA were systematically studied. Based on electron microscopy analysis, we found the intercalation of CNT into the rGO sheets can form a rich porous structure, which provides open channels for ion transport and reduces ion diffusion resistance. Meanwhile, CNT 'soldered' in-between rGO sheets can avoid the slip of cellular layers under compression, which offers the as-prepared aerogels super-elasticity. During the hydrothermal reduction of GO sheets, an efficient self-assembly process is triggered as a result of hydrophobic π-π stacking interactions between rGO and SWCNTs. We found the hydrophilic and hydrophobic transition of GO is originated from the partially hydrothermal reduction reaction, which eliminates the surface-functionalised oxygen-containing moieties during the formation of rGO. Additionally, the electrochemical impedance spectroscopy (EIS)

results prove that the addition of CNT can dramatically improve the electrical conductivity of GCA. In the end, electrochemical measurements show that GCA 2-2 SCs display excellent gravimetric capacitance of 117 $F \cdot g^{-1}$ at a discharge current density of 1 $A \cdot g^{-1}$, which can provide a high energy density of 3.53 $Wh \cdot kg^{-1}$ at a power density of 238.4 $kW \cdot kg^{-1}$ for our as-prepared symmetrical supercapacitor. Our findings elucidate the ratio-dependent electrochemical performance between GO, reduced GO (graphene), CNT and self-organised GCA, which offers practical guidance of assembling 2D materials into 3D aerogels for ultra-flyweight electrochemical energy storage applications.

MATERIALS AND METHODS

Preparation of GO. GO was prepared via a modified Hummers approach[30] from natural graphite flake (Graphite was purchased from Aladdin Industrial Corporation with 1200 mesh, purity > 99.95%). Typically, a 9:1 mixture of concentrated acids (180 mL H_2SO_4: 20 mL H_3PO_4) was added into a flask with 1.5 g of graphite at room temperature. 9.0 g of $KMnO_4$ powder was gradually added into the graphite suspension solution under vigorous stirring to keep the temperature under 30 ℃. The reaction mixture was held at 50 °C for a 12 h, and then the reaction was quenched by adding 200 mL of ice water into the reaction solution together with an ice bath. Furthermore, 30% of H_2O_2 was dropwise added to the reaction solution to remove excess $KMnO_4$. The resultant bright yellow dispersion was centrifuged and washed with 10% HCl aqueous solution to remove metal ions, followed by repeated centrifugation and washing with distilled water to remove the acidic residues until the solution is neutral. Pure GO solid was obtained by further centrifugation and drying at 80 °C for two days.

Acidification of CNT. 400 mg of single-walled carbon nanotubes (SWCNT was purchased from Aladdin Industrial Corporation, purity > 95%, external diameter: < 2 nm, length: 0.3~5 μm) were dispersed into 160 mL H_2SO_4 and HNO_3 mixture (3:1 v/v) in a 500 mL beaker. The mixture was subsequently sonicated for 4 h at room temperature and then diluted by slowing adding of 200 ml of distilled water (at this point, the mixture will become a suspension, which is convenient for filtration). Later, the resulting product was recovered from the suspension by filtration and washing with distilled water and acetone several times to remove the acidic residues. In the end, the product of CNT was collected by drying at 80 °C for 24 h.

Preparation of rGO/CNT aerogels (GCA) electrode. The preparation process was schematically illustrated in Figure1a. Typically, a series of GO dispersion with a concentration of 2, 3, and 4 $mg{\cdot}mL^{-1}$ was prepared by dispersing GO powder into deionised water under continuous sonication (KQ-300VDE, 45 kHz, 8 h). Because of the difficulties of dispersing CNT powder into deionised water, we prepared 2 $mg{\cdot}mL^{-1}$ CNT dispersion in N, N-Dimethylformamide (DMF) under 8 h sonication. Then, CNT dispersion was added into GO dispersion with a volume ratio of H_2O: DMF = 9:1 (this is the optimal ratio for hydrogel moulding, Figure S1), and the mixture was further sonicated for 30 min to produce a homogeneous dispersion. rGO/CNT hydrogel was formed by self-assembly of GO sheets and CNT using a hydrothermal reduction approach under 180 °C for 4 h in a Teflon-lined autoclave. After naturally cooling down to room temperature, the received rGO/CNT hydrogels were immersed in deionised water for two days, during which deionised water was changed every 12 h to remove DMF. After freezing the hydrogels in refrigerator for 24 h, following with freeze-drying for 2 days, the rGO/CNT aerogels were produced. The as-prepared rGO/CNT

aerogels were defined as GCA 4-2, GCA 3-2, and GCA 2-2 based on the concentration ratio of pristine GO to CNT (e.g. 4 $mg \cdot mL^{-1}$ GO dispersion mixing with 2 $mg \cdot mL^{-1}$ CNT dispersion defined as GCA 4-2). Also, GO/CNT aerogels were also made by changing the concentration of CNT dispersion without GO hydrothermal reduction, and the specific naming correspondence and the mass ratio of GO to CNT are listed in Table S1. A pure graphene aerogel (GA) without CNT was also prepared under the same approach (3 $mg \cdot mL^{-1}$ GO dispersion was employed in this process).

The working electrode was prepared as follows: aerogels (electroactive material), polyvinylidene fluoride (PVDF, binder) and carbon black (conductive agent) were mixed with N-methyl-2-pyrrolidone (NMP) solvent to form a homogeneous slurry with a weight ratio of 8:1:1. This slurry was coated onto the nickel foam substrate (1×1 cm) and dried at 80 °C for 12 h, and then pressed at a pressure of 10 MPa to form a thin sheet. The mass of the active material on one electrode is about 5 $mg \cdot cm^{-2}$.

Structure and morphology characterization. The morphological structure of the aerogels was investigated by an FEI-Quanta 250 FEG scanning electron microscopy (SEM, FEI, Hillsboro, USA) with 10 kV operating voltage. Transmission electron microscopy (TEM) images were acquired using HT7700 microscopy (Hitachi, Ltd., Chiyoda, Japan). Fourier transform infrared spectroscopy was employed to identify the functional groups on the materials by a Nicolet Avatar 360 FT-IR spectroscopy (FT-IR, Instrument Co., Madison, WI,

USA). Raman spectroscopy analysis was carried out on a dried solid with an excitation wavelength of 532 nm (LabRAM HR Evolution, HORIBA Jobin Yvon, France). X-ray diffraction (XRD) patterns were collected on Rigaku MiniFlex 600 X-ray diffractometer (Rigaku Co., Tokyo, Japan) with Cu Kα radiation over the 2θ range of 5°−80°. X-ray photoelectron spectroscopy (XPS) measurements were carried out on K-alpha (Thermo Scientific Inc. U.K). The N_2 adsorption/desorption isotherms were measured via ASAP 2020 HD88 (Micromeritics Instrument Corp., USA) at 77K. The electrical conductivity was measured by an RTS-9 (4 PROBES TECH, Guangzhou, China) four-point probes station.

Electrochemical measurements. All electrochemical measurements were performed on a CHI660E electrochemical workstation (Shanghai Chen Hua Instruments Co., Shanghai, China). All the tests were carried out in a three-electrode cell consisted of the as-prepared carbon aerogels electrode as the working electrode, a 2 cm × 2 cm Pt sheet as the counter electrode, Ag/AgCl (saturated KCl) as the reference electrode, and 1 M Na_2SO_4 aqueous solution as the electrolyte. Cyclic voltammograms (CV) curves were recorded at a scan rate of 10 $mV \cdot s^{-1}$ with a potential window of 0-1 V. Electrochemical impedance spectroscopy (EIS) measurements were measured in a frequency range from 10^{-2}-10^5 Hz with ac amplitude of 5 mV at open circuit potential. Galvanostatic charge-discharge (GCD) tests were performed at a current of 1, 2, 4, 6, 8, 10, 15, 20 $A \cdot g^{-1}$ with a cut-off voltage of 0-1 V.

The gravimetric specific capacitance (C_s) was calculated from the GCD discharge curves using

the following equation: C_s ($F \cdot g^{-1}$) = $I \cdot \Delta t/(m \cdot \Delta U)$, where I is the discharging current (A), Δt is the discharging time (s), m is the mass of active material on one electrode (g), and ΔU (V) is the potential discharging range.

The symmetric supercapacitor (SC) was fabricated with a 1.0 M Na_2SO_4 aqueous solution to evaluate the energy density. Two GCA 2-2 electrodes were immersed in 1.0 M Na_2SO_4 aqueous solution for 12 h and then separated by filter paper soaked with electrolyte. The GCD test was performed at a current density of 2 $A \cdot g^{-1}$ with a potential range of 0-1 V. The gravimetric specific capacitance (C_s) was calculated based on the total mass of two electrodes: C_s ($F \cdot g^{-1}$) = $4I \cdot \Delta t/(m \cdot \Delta U)$ and C_s ($F \cdot g^{-1}$) = $\int I(U)dU/(2 \cdot m \cdot \upsilon \cdot \Delta U)$, where υ is the scan rate ($V \cdot s^{-1}$).

RESULTS AND DISCUSSION

The fabrication process of the GCA is described schematically in Figure 1a. It can be seen that GO has a hydrophilic surface property and dispersible in water which is resulted from oxygen-containing functional groups on its surface.[10] In order to realize a homogeneous miscible solution between hydrophilic GO and hydrophobic CNTs, a co-solvent mixing strategy is employed, where CNT powders are dispersed into DMF prior to the hybridization with GO in water solution. We found a volume ratio of H_2O: DMF = 9:1 is the optimal ratio to obtain a homogeneous dispersion between GO and CNTs. During the reduction of GO sheets in the autoclave at hydrothermal conditions, GO was partially reduced to rGO, and the surface polarity subsequently changed to hydrophobic. Thus, efficient self-assembly occurs as a result of

hydrophobic and π-π stacking interactions between rGO and CNT.[31] Based on the steric hindrance effect of graphene sheets, a 3D porous structure of graphene can be formed. The microstructure of CNT, GO, rGO, rGO/CNT hydrogel, and rGO/CNT hydrogel (GCA) are shown in Figure 1b. Because of the porous structure of aerogel, it has a relatively low density (14.3 $kg \cdot m^{-3}$ for GCA 2-2, see Figure S2). However, the main contribution to its specific surface area is the microporous structure of CNT itself and the micropores formed by the stacking of rGO sheets and CNT. As shown in Figure S3, the pore size ranges from 1 to 10 nm. Pore structure parameters of GCA 2-2 are listed in Table S2 and the Brunauer-Emmett-Teller (BET) specific surface areas of GCA 2-2 and GCA 3-2 are calculated to be 259.7 and 223.0 $m^2 \cdot g^{-1}$, respectively.

The microstructure of GA which made from GO-only was also characterised through SEM analysis. Figure 2a shows that the GA has a randomly lapped three-dimensional (3D) framework with continuous macropores. An enlarged micrograph reveals crinkly ultrathin GO sheet, which suggests GO is well dispersed (Figure 2b) in as-prepared GA. Due to the existence of a large number of carboxyl and hydroxyl groups (Figure 1b), the GO sheet is negatively charged in the aqueous dispersion which prevents them from aggregation.[32-34] On the other hand, the alternation of surface polarity of GO sheets shall significantly affect its solubility due to the changing of their electrostatic repulsion.[32-34]

The morphological structures of GCA with different CNT contents are analysed via SEM and

TEM, as shown in Figure 3(a-c), Figure S4, Figure S5 and Figure S6 (the mass ratio of GO to CNT was listed in Table S1). As shown in the TEM images (Figure S6), the interconnected structure and the cell dimension changed dramatically after introducing CNT into GO monoliths. Different forms of interconnection structures have also been resolved under high-resolution SEM analysis such as semi-curling for GCA 4-2 (Figure 3d), bending for GCA 3-2 (Figure 3e) and scrolling for GCA 2-2 (Figure 3f). The corresponding cartoons of CNT-intercalated GO building block and its geometrical interconnections are shown in Figure 3g-i. The other forms of the interconnections such as overlapping (Figure S7 a,d), tearing (Figure S7b, e), and enwrapping (Figure S7c, f) are shown in Figure S7. It is worth noting that, in Figure 3 (d-f), these aligned CNTs intercalated into rGO layers not only suppress the further-accumulation of rGO stacking sheets but also provide good porosity in the hybrids associated with the maximum utilisation of CNT.[35-36] It should be noted that as-prepared neat GA without CNT is frangible and has no elasticity, while GCA has excellent flexibility (Figure 3j).

FTIR was employed to identify the changing of surface functional groups on the electrode materials. Similar characteristic absorption peaks are observed in the spectra of all aerogels. As shown in Figure 4a and Figure S8, the peaks located at 3460 cm^{-1} and 1630 cm^{-1} are attributed to O−H hydroxyl stretching vibrations of adsorbed water. The presence of carboxylic acid functional groups was confirmed by the O−H stretching vibrations peak at 3230 cm^{-1}, C=O stretching vibrations peak at 1790 cm^{-1}, and C-O stretching vibrations peak at 1320 cm^{-1}. The other signals such as 3580, 2890, 1440, 1180, 990, and 680-880 cm^{-1} correspond to O−H hydroxyl stretching vibration, C−H stretching vibration, C=C stretching vibration of the

benzene ring, C−O epoxy stretching vibration, C−O alkoxy stretching vibration, and C−H out-of-plane bending vibration of aromatic ring.[10] It can be observed that signals in the spectrum of GCA 2-2 are weaker than the others, which indicate the elimination of oxygen moieties and a different stacking mode between GO and CNT shall be presented (as shown in Figure 3f).

Raman spectroscopy was used to further investigate the structural changes of aerogels as a function of the CNT intercalation. Figure 4b shows the Raman spectra of GA, GCA4-2, GCA3-2, and GCA2-2 aerogels. The G-band at around 1590 cm^{-1} is attributed to the vibration of sp^2 hybrid carbon atoms in a hexagonal lattice (such as in a graphene sheet or CNT), and the D-band at about 1340 cm^{-1} is usually associated with the defect or disorder structure.[37-38] The peak intensity ratio of D-band and G-band (I_D/I_G) of GA was calculated to be 1.021, which is considerably higher than those of GCA4-2 (0.093), GCA3-2 (0.068), and GCA2-2 (0.113). Large I_D/I_G value indicates GA has a high disorder degree in sp^2 carbon.[37-39] After intercalation of CNT, I_D/I_G value drops dramatically, which is attributed to the higher peak intensity of CNT than GA. Compared with other GCA aerogels, GCA3-2 shows the lowest I_D/I_G value of 0.068, which indicate that GCA3-2 has the most ordered structure.[37, 39-40] This result is consistent with the SEM results shown in Figure 3(d-f). There is a 2D-band peak has also been observed in all samples. GO usually stack together owing to the interlayer hydrogen bonding, so GA (GO aerogel) has weak and broad 2D peaks.[41] In comparison, in all GCA samples, an enhanced 2D-band peak can be observed, which suggests that the addition of CNT can effectively prevent the attacking of GO sheets.

To better understand the crystal structure of GCA materials, the XRD analysis of Gt (natural graphite), GO, CNT, and GA was performed and shown in Figure 5a. The characteristic peak at 26.4° is owing to the (002) crystal plane of Gt with an interlayer spacing of 0.34 nm. For GO sample, the (002) diffraction peak is shifted to 2θ = 9.4° (d = 0.94 nm) after chemical oxidation. It indicates that the introduction of oxygen moieties can function effectively and separate the GO sheets.[35] After the hydrothermal reaction, a broad diffraction peak at 2θ = 24.0° (d = 0.370 nm) is observed, which is attributed to the (002) crystal plane of graphitic carbon in GA. The decrease of interlayer distance suggests that GO was successfully reduced by the depletion of oxygen, and the broader peaks indicated high stacking disorder.[42] Figure 5b shows the XRD patterns of GO/CNT hybrid aerogel (GCA) as a function of their mass ratios for GCA4-2 is 18:1, GCA3-2 is 13.5:1, and GCA2-2 is 9:1, respectively (XRD patterns of the other aerogels are shown in Figure S9). For GCA samples, a broad peak was observed at 2θ = 24.7°, indicates the stacking disorder of GO sheets along their stacking direction and reflects that the framework of the GCA is formed by stacking a few-layer GO sheets and CNT. The appearance of the sharp peaks at 22.2° and 26.5° in the XRD patterns of GCA4-2 and GCA3-2, indicates a strong stacking between GO layers and CNT, and the degree of graphitisation increased[22], which is consistent with the SEM results.

XPS spectra of GA and GCA2-2 are shown in Figure 5c. The contents of C and O elements are 83.76% and 16.24% for GA, 85.6% and 14.4% for GCA2-2. The presence of CNT reduced the content of O in GCA2-2. The C1s spectra of GA (Figure 5e) and GCA2-2 (Figure 5f) were divided into four main peaks centered at 284.1, 285.5, 287.8 and 289.8 eV corresponding to C-

C/C=C, C-OH, C=O and O-C=O bonds, respectively. As shown in Figure 5d, the O1s spectra mainly divided into three peaks with binding energies of 530.6, 532.5 and 535.3 for GA, and 531.1, 533.0 and 534.3 for GCA2-2. These peaks attributed to C=O, O-C=O and C-O bonds, respectively. The O1s spectrum of GCA2-2 shows significant changes owing to the presence of CNT. The content of C=O bonds increased significantly, while O-C=O bonds decreased, indicating O-C=O is the main oxygen-containing functional groups in GA.

To investigate the performance of supercapacitor electrode based on GO/CNT aerogels, cyclic voltammetry (CV), electrochemical impedance spectroscopy (EIS) and galvanostatic charge/discharge (GCD) analysis were performed with a three-electrode system in 1 $mol \cdot L^{-1}$ Na_2SO_4 aqueous solution. As shown in Figure 6a, owing to its fast charge transfer and ion diffusion within the electrodes, CNT showed a quasi-rectangular shape CV curves. The appearance of the slight hump indicates the existence of pseudo-capacitance which may be originated from the oxygen functional groups on carbon materials such as hydroxyls and carboxyls.[43-44] For the GA electrode, though GA electrode shows a larger integral area than GO electrode, its CV curves considerably deviate from rectangle which was due to the inferior ion diffusion and poor electrical conductivity caused by the stacking of GO sheets.[45] Figure 6b shows the CV curves of a series of GCA electrodes with different rGO/CNT mass ratio. With the increase of the content of CNT, the CV curve is getting closer to the rectangular shape, and the loop area is increased, which attributes to the CNT-mediated fast ion transfer as well as high electrical conductivity.[10]

To further investigate the ion transport and electron transfer dynamics, EIS analysis was carried out on the electrodes. Nyquist plots of GO, GA, CNT and GCA electrodes are shown in Figure 6c and d and Figure 6e, respectively. The fitting results showed that the values of R_{ct} for GO, GA, and CNT electrodes are 742.6, 25.6 and 0.34 Ω, respectively (Figure S10 and Figure S11). Compare with GO electrode, GA shows a much smaller R_{ct} and a more vertical tail means a faster charge transfer and excellent capacitive behaviour. In addition, a CNT electrode has the smallest R_{ct}, which means it has the quickest charge transfer rate and the highest electrical conductivity. As shown in Figure 6e, the R_{ct} is monotonically decreasing with CNT loading, which indicates an improvement of electrical conductivity in GCA electrodes. The fitting results are shown in Figure S11, and the values of R_{ct} are 10.9, 9.36 and 7.62 Ω for GCA 4-2, GCA 3-2, and GCA 2-2, respectively. These results are consistent with four-probe electrical conductivity test (Figure S12, and Table S3), which shows the sheet resistance of GCA 4-2, GCA 3-2, and GCA 2-2 are 0.5, 1.0 and 1.33 $S \cdot cm^{-1}$, respectively. Moreover, the Warburg impedance of GCA electrodes was much smaller than that of GA, indicates the improved ion-diffusion upon the addition of CNT. To better analyse the frequency response of the electrode, the relaxation time constant t_0 was calculated, as shown in Figure 6h. t_0 represents the minimum time required to discharge the stored energy with 50% efficiency.[46] Compare with the other GCA electrodes, GCA 2-2 exhibited the smallest t_0 of 14.7 s, indicates the fastest charge-discharge characteristics and the most facile penetration of ions into pores.

The GCD curves of GO, GA, CNT, and GCA at a current density of 2 $A \cdot g^{-1}$ are shown in Figure 7a and Figure 7b, which reveal the electrochemical double-layer capacitive behaviour of these

electrodes. Generally, the discharge time is indicative of the specific capacitance of the active material at the same current density.[47] It can be seen that GCA 2-2 exhibited extended charging and discharging time as well as small "IR drop" (isosceles triangle shape), suggesting that the addition of CNT improved the energy storage and the power performance.[42] The calculated specific capacitance values of all electrodes were shown in Figure 7c, and d. As the current density increases from 1 to 10 $A \cdot g^{-1}$, GA and GCA 2-2 maintain 14% (from 171.8 $F \cdot g^{-1}$ to 23.0 $F \cdot g^{-1}$) and 57% (from 130.5 $F \cdot g^{-1}$ to 73.7 $F \cdot g^{-1}$) of their initial capacitances, indicate that GCA 2-2 has better rate capability than GA. It should be noted that compared to monolayer Graphene, GO has many defective structures, which results in the 'sudden drop' of the capacitance when increasing current density.[31, 42, 48-49] Thus, the GCA 2-2 electrode was selected to test the cycling stability. As shown in Figure 7e, the capacitance retentions of GCA 2-2 was about 61% over 2,000 cycles at 2 $A \cdot g^{-1}$, and the Coulombic efficiency reaches nearly 100%.

To further investigate the electrochemical stability of GCA 2-2 electrode, symmetrical supercapacitor (GCA2-2//GCA2-2) was assembled and evaluated in 1 M Na_2SO_4 aqueous electrolyte. The symmetrical supercapacitor cross-section configuration is shown in Figure 8a. It should be noted that the as-prepared GCA 2-2 electrode exhibits good mechanical stability. As shown in Figure S13, the microporous structure can well remain after the device fabrication. Figure 8b show the CV curves at various scan rates between 5 $mV \cdot s^{-1}$ and 100 $mV \cdot s^{-1}$. The rectangular shape of the CV curves indicates the ideal capacitive behavior of the electrodes. Figure 8c shows the effects of scan rates on the specific capacitance of GCA2-2//GCA2-2 symmetrical supercapacitor. The result shows that the specific capacitance of the device is

almost 1/4 of that of a single electrode. As showed in Figure 8d, a highly symmetrical GCD curve can be revealed at a current density of 0.5-20 $A \cdot g^{-1}$, which indicates excellent electrochemical reversibility. The specific capacitances of 26.5, 25.45, 23.8, 21, 18.6, 16.2, 15.1, 12.75, 11 $F \cdot g^{-1}$ were calculated based on the discharge time at a current density of 0.5, 1, 2, 4, 6, 8, 10, 15, 20 $A \cdot g^{-1}$ (Figure 8d and Figure 8e), respectively. As shown in Figure S14, the Ragone plots of the assembled symmetric supercapacitor exhibit an energy density of 3.53 $Wh \cdot kg^{-1}$ at a power density of 283.4 $W \cdot kg^{-1}$. A minimal IR drop (~ 0.05 V) was observed at a current density of 1 $A \cdot g^{-1}$, which suggests low internal resistance for the GCA 2-2 electrodes. The relaxation time constant t_0 of the device is 31.6 s (Figure 8f), which is very close to that of one single electrode, which indicates fast charge-discharge characteristics. Meanwhile, there is only one peak was observed in Figure 8f, which indicates that there is only one primary charge storage mechanism, which is more likely due to ion adsorption.[50]

CONCLUSIONS

In summary, we elucidate the ratio-dependent electrochemical performance between GO, reduced GO (graphene), CNT and self-organised GCA, which offers practical guidance of assembling 2D materials into 3D aerogels. GCA was designed and synthesised via controlling the hydrophobic and hydrophilic transition during hydrothermal reduction. The addition of CNT greatly enhanced electrical conductivity and mechanical durability of GCA, which shows a much smaller charge transfer resistance (7.62 Ω) than conventional GA (25.6 Ω). In addition, the presence of CNT in the aerogel effectively prevents the collapse of the 3D framework of

GA and improves the rate performance and cycle stability of GA electrode. The GCA 2-2 based symmetrical supercapacitor delivered an excellent energy density of 3.53 $Wh \cdot kg^{-1}$ at a power density of 283.4 $W \cdot kg^{-1}$ and 1.53 $Wh \cdot kg^{-1}$ at a power density of 6875 $W \cdot kg^{-1}$. The GCA 2-2 based symmetrical supercapacitor shows a relaxation time constant t_0 of 31.6 s, which is very close to that of one single electrode, indicating fast charge-discharge characteristics. These findings are an essential step towards a new approach for addressing the fundamental challenge of low conductivity and collapsible 2D assembled cellular aerogels. Various ultra-flyweight electrochemical energy storage devices with the already reported properties and preparation methods can be envisioned.

ASSOCIATE CONTENT

Supporting information

Digital photographs of graphene oxide/carbon nanotube hydrogel, the specific naming correspondence and the mass ratio of GO to CNT, digital photographs of GCA 2-2 and the calculation method of density, N_2 adsorption and desorption isotherms and pore size distribution, pore structure parameters of GCA 2-2 and GCA 3-2, additional SEM and TEM images of sample GCA 2-2, SEM images of different interconnections for CNTs-intercalated GO cell walls, FTIR, XRD, additional EIS spectra analysis results, four-point probe conductivity analysis results, SEM cross-section images from disassembled symmetrical supercapacitors and the Ragone plot of GCA 2-2.

AUTHOR INFORMATION

Corresponding author

Email: HouB6@cardiff.ac.uk, Tel: +44 (0)29 22510756. (Bo Hou)

ORCID

Mingxia Lu: https://orcid.org/0000-0001-6574-0374

Jingchao Zhang: https://orcid.org/0000-0001-5289-6062

Zhe Li: https://orcid.org/0000-0002-7404-7448

Bo Hou: https://orcid.org/0000-0001-9918-8223

Author contributions

M.L. and B.H. conceived the experiments and led the project. M.L. and S.L. performed material synthesis, device fabrication, and characterisation. J.C., X.Z., J.Z. and Z.L. contributed to scientific discussion and provided experimental guidance. M.L., X.Z. and B.H. contributed to the interpretation of the data and commented on the manuscript. M.L. and B.H. wrote the paper with input and discussion from all authors.

ACKNOWLEDGMENTS

This work was supported by the PhD Programs Foundation of the Henan University of Technology (No. 31401546). Fundamental Research Funds for the Henan Provincial Colleges and Universities, China (No. 2016NQJH06). The Science and Technology Foundation of Henan Province (No. 192102210044, No.192102210170). Key Scientific and Technological

Research Projects of Henan Education Committee (No. 14B430005). B.H. also would like to acknowledge the financial support by the Cardiff University.

REFERENCES

1. Someya, T.; Bao, Z.; Malliaras, G. G. The Rise of Plastic Bioelectronics. *Nature* **2016**, *540*, 379-385.
2. Pazhamalai, P.; Krishnamoorthy, K.; Sahoo, S.; Mariappan, V. K.; Kim, S.-J. Carbothermal Conversion of Siloxene Sheets into Silicon-Oxy-Carbide Lamellae for High-Performance Supercapacitors. *Chem. Eng. J.* **2020**, *387*, 123886.
3. Xia, L.; Li, X.; Wu, Y.; Hu, S.; Liao, Y.; Huang, L.; Qing, Y.; Lu, X. Electrodes Derived from Carbon Fiber-Reinforced Cellulose Nanofiber/Multiwalled Carbon Nanotube Hybrid Aerogels for High-Energy Flexible Asymmetric Supercapacitors. *Chem. Eng. J.* **2020**, *379*, 122325.
4. Kim, D. W.; Jung, S. M.; Jung, H. Y. A Super-Thermostable, Flexible Supercapacitor for Ultralight and High Performance Devices. *J. Mater. Chem. A* **2020**, *8*, 532-542.
5. Wang, L.; Fu, X.; He, J.; Shi, X.; Chen, T.; Chen, P.; Wang, B.; Peng, H. Application Challenges in Fiber and Textile Electronics. *Adv. Mater.* **2019**, *32*, 1901971.
6. Chen, T.; Dai, L. Flexible Supercapacitors Based on Carbon Nanomaterials. *J. Mater. Chem. A* **2014**, *2*, 10756-10775.
7. Wang, Q.; Ma, Y.; Liang, X.; Zhang, D.; Miao, M. Flexible Supercapacitors Based on Carbon Nanotube-MnO_2 Nanocomposite Film Electrode. *Chem. Eng. J.* **2019**, *371*, 145-153.
8. Yuan, L.; Lu, X.-H.; Xiao, X.; Zhai, T.; Dai, J.; Zhang, F.; Hu, B.; Wang, X.; Gong, L.; Chen, J., et al. Flexible Solid-State Supercapacitors Based on Carbon Nanoparticles /MnO_2 Nanorods Hybrid Structure. *ACS Nano* **2012**, *6*, 656-661.
9. Ghosh, A.; Lee, Y. H. Carbon-Based Electrochemical Capacitors. *ChemSusChem* **2012**, *5*, 480-499.
10. Lu, M.; Wang, G.; Li, B.; Chen, J.; Zhang, J.; Li, Z.; Hou, B. Molecular Interaction Balanced One- and Two-Dimensional Hybrid Nanoarchitectures for High-Performance Supercapacitors. *Phys. Chem. Chem. Phys.* **2019**, *21*, 22283-22292.
11. Xu, Y.; Shi, G.; Duan, X. Self-Assembled Three-Dimensional Graphene Macrostructures: Synthesis and Applications in Supercapacitors. *Accounts Chem. Res.* **2015**, *48*, 1666-1675.
12. Yang, X.; Cheng, C.; Wang, Y.; Qiu, L.; Li, D. Liquid-Mediated Dense Integration of Graphene Materials for Compact Capacitive Energy Storage. *Science* **2013**, *341*, 534-537.
13. Zhu, Y., et al. Carbon-Based Supercapacitors Produced by Activation of Graphene. *Science* **2011**, *332*, 1537-1541.
14. He, N.; Yildiz, O.; Pan, Q.; Zhu, J.; Zhang, X.; Bradford, P. D.; Gao, W. Pyrolytic-Carbon Coating in Carbon Nanotube Foams for Better Performance in Supercapacitors. *J. Power Sources* **2017**, *343*, 492-501.
15. Honda, Y.; Haramoto, T.; Takeshige, M.; Shiozaki, H.; Kitamura, T.; Ishikawa, M. Aligned MWCNT Sheet Electrodes Prepared by Transfer Methodology Providing High-Power

Capacitor Performance. *Electrochem. Solid St.* **2007**, *10*, A106-A110.
16. Yoshio, M.; Nakamura, H.; Wang, H. Novel Megalo-Capacitance Capacitor Based on Graphitic Carbon Cathode. *Electrochemical and Solid-State Letters* **2006**, *9*, A561-A563.
17. Wang, G.; Zhang, L.; Zhang, J. A Review of Electrode Materials for Electrochemical Supercapacitors. *Chem. Soc. Rev.* **2012**, *41*, 797-828.
18. Salanne, M.; Rotenberg, B.; Naoi, K.; Kaneko, K.; Taberna, P. L.; Grey, C. P.; Dunn, B.; Simon, P. Efficient Storage Mechanisms for Building Better Supercapacitors. *Nat. Energy* **2016**, *1*, 16070.
19. Sun, H.; Xu, Z.; Gao, C. Multifunctional, Ultra-Flyweight, Synergistically Assembled Carbon Aerogels. *Adv. Mater.***2013**, *25*, 2554-2560.
20. Ji, J.; Li, Y.; Peng, W.; Zhang, G.; Zhang, F.; Fan, X. Advanced Graphene-Based Binder-Free Electrodes for High-Performance Energy Storage. *Adv. Mater.* **2015**, *27*, 5264-5279.
21. Worsley, M. A.; Pauzauskie, P. J.; Olson, T. Y.; Biener, J.; Satcher, J. H.; Baumann, T. F. Synthesis of Graphene Aerogel with High Electrical Conductivity. *J. Am. Chem. Soc.* **2010**, *132*, 14067-14069.
22. Xu, Y.; Sheng, K.; Li, C.; Shi, G. Self-Assembled Graphene Hydrogel via a One-Step Hydrothermal Process. *ACS Nano* **2010**, *4*, 4324-4330.
23. Kim, J.; Cote, L. J.; Kim, F.; Yuan, W.; Shull, K. R.; Huang, J. Graphene Oxide Sheets at Interfaces. *J. Am. Chem. Soc.* **2010**, *132*, 8180-8186.
24. Shao, J.-J.; Lv, W.; Yang, Q.-H. Self-Assembly of Graphene Oxide at Interfaces. *Adv. Mater.* **2014**, *26*, 5586-5612.
25. Ma, Z.; Zhao, X.; Gong, C.; Zhang, J.; Zhang, J.; Gu, X.; Tong, L.; Zhou, J.; Zhang, Z. Preparation of a Graphene-Based Composite Aerogel and the Effects of Carbon Nanotubes on Preserving the Porous Structure of the Aerogel and Improving Its Capacitor Performance. *J. Mater. Chem. A* **2015**, *3*, 13445-13452.
26. Lv, P.; Tan, X.-W.; Yu, K.-H.; Zheng, R.-L.; Zheng, J.-J.; Wei, W. Super-Elastic Graphene/Carbon Nanotube Aerogel: A Novel Thermal Interface Material with Highly Thermal Transport Properties. *Carbon* **2016**, *99*, 222-228.
27. Zheng, Q.; Cai, Z.; Ma, Z.; Gong, S. Cellulose Nanofibril/Reduced Graphene Oxide/Carbon Nanotube Hybrid Aerogels for Highly Flexible and All-Solid-State Supercapacitors. *ACS Appl. Mater. Inter.* **2015**, *7*, 3263-3271.
28. Lu, M.; Ohba, T.; Kaneko, K.; Hata, K.; Yumura, M.; Iijima, S.; Komatsu, H.; Sakuma, A.; Kanoh, H. Electron Density Modification of Single Wall Carbon Nanotubes (SWCNT) by Liquid-Phase Molecular Adsorption of Hexaiodobenzene. *Materials* **2013**, *6*, 535-543.
29. Cheng, C.; Li, S.; Thomas, A.; Kotov, N. A.; Haag, R. Functional Graphene Nanomaterials Based Architectures: Biointeractions, Fabrications, and Emerging Biological Applications. *Chem. Rev.* **2017**, *117*, 1826-1914.
30. Gilje, S.; Han, S.; Wang, M.; Wang, K. L.; Kaner, R. B. A Chemical Route to Graphene for Device Applications. *Nano Lett.* **2007**, *7*, 3394-3398.
31. Jokar, E.; Shahrokhian, S.; zad, A. I.; Asadian, E.; Hosseini, H. An Efficient Two-Step Approach for Improvement of Graphene Aerogel Characteristics in Preparation of Supercapacitor Electrodes. *J. Energy Storage* **2018**, *17*, 465-473.
32. Kim, B.; Park, H.; Sigmund, W. M. Electrostatic Interactions between Shortened Multiwall Carbon Nanotubes and Polyelectrolytes. *Langmuir* **2003**, *19*, 2525-2527.

33. Yu, D.; Dai, L. Self-Assembled Graphene/Carbon Nanotube Hybrid Films for Supercapacitors. *J. Phys. Chem. Lett.* **2010**, *1*, 467-470.
34. Tan, Y.; Wu, D.; Wang, T.; Liu, P.; Guo, J.; Jia, D. Facile Synthesis of Functionalized Graphene Hydrogel for High Performance Supercapacitor with High Volumetric Capacitance and Ultralong Cycling Stability. *Appl. Surf. Sci.* **2018**, *455*, 683-695.
35. Gunjakar, J. L.; Hou, B.; Inamdar, A. I.; Pawar, S. M.; Abu Talha, A. A.; Chavan, H. S.; Kim, J.; Cho, S.; Lee, S.; Jo, Y., et al. Two-Dimensional Layered Hydroxide Nanoporous Nanohybrids Pillared with Zero-Dimensional Polyoxovanadate Nanoclusters for Enhanced Water Oxidation Catalysis. *Small* **2018**, *14*, 1703481.
36. Gunjakar, J. L.; Inamdar, A. I.; Hou, B.; Cha, S.; Pawar, S. M.; Abu Talha, A. A.; Chavan, H. S.; Kim, J.; Cho, S.; Lee, S., et al. Direct Growth of 2d Nickel Hydroxide Nanosheets Intercalated with Polyoxovanadate Anions as a Binder-Free Supercapacitor Electrode. *Nanoscale* **2018**, *10*, 8953-8961.
37. Ferrari, A. C.; Meyer, J. C.; Scardaci, V.; Casiraghi, C.; Lazzeri, M.; Mauri, F.; Piscanec, S.; Jiang, D.; Novoselov, K. S.; Roth, S., et al. Raman Spectrum of Graphene and Graphene Layers. *Phys.Rev. Lett.* **2006**, *97*, 187401.
38. Aboutalebi, S. H.; Chidembo, A. T.; Salari, M.; Konstantinov, K.; Wexler, D.; Liu, H. K.; Dou, S. X. Comparison of GO, GO/MWCNTs Composite and MWCNTs as Potential Electrode Materials for Supercapacitors. *Energ. Environ. Sci.* **2011**, *4*, 1855-1865.
39. Saito, R.; Hofmann, M.; Dresselhaus, G.; Jorio, A.; Dresselhaus, M. S. Raman Spectroscopy of Graphene and Carbon Nanotubes. *Adv. Phys.* **2011**, *60*, 413-550.
40. Ferrari, A. C. Raman Spectroscopy of Graphene and Graphite: Disorder, Electron–Phonon Coupling, Doping and Nonadiabatic Effects. *Solid State Commun.* **2007**, *143*, 47-57.
41. Dreyer, D. R.; Park, S.; Bielawski, C. W.; Ruoff, R. S. The Chemistry of Graphene Oxide. *Chem. Soc. Rev.* **2010**, *39*, 228-240.
42. Cui, X.; Lv, R.; Sagar, R. U. R.; Liu, C.; Zhang, Z. Reduced Graphene Oxide/Carbon Nanotube Hybrid Film as High Performance Negative Electrode for Supercapacitor. *Electrochim. Acta* **2015**, *169,* 342-350.
43. Li, X.; Rong, J.; Wei, B. Electrochemical Behavior of Single-Walled Carbon Nanotube Supercapacitors under Compressive Stress. *ACS Nano* **2010**, *4*, 6039-6049.
44. Bichat, M. P.; Raymundo-Piñero, E.; Béguin, F. High Voltage Supercapacitor Built with Seaweed Carbons in Neutral Aqueous Electrolyte. *Carbon* **2010**, *48*, 4351-4361.
45. Stoller, M. D.; Ruoff, R. S. Best Practice Methods for Determining an Electrode Material's Performance for Ultracapacitors. *Energ. Environ. Sci.* **2010**, *3*, 1294-1301.
46. Taberna, P. L.; Simon, P.; Fauvarque, J. F. Electrochemical Characteristics and Impedance Spectroscopy Studies of Carbon-Carbon Supercapacitors. *J. Electrochem. Soc.* **2003**, *150*, A292-A300.
47. Ling, Z.; Wang, G.; Dong, Q.; Qian, B.; Zhang, M.; Li, C.; Qiu, J. An Ionic Liquid Template Approach to Graphene–Carbon Xerogel Composites for Supercapacitors with Enhanced Performance. *J. Mater. Chem. A* **2014**, *2*, 14329-14333.
48. Mao, X.; Xu, J.; He, X.; Yang, W.; Yang, Y.; Xu, L.; Zhao, Y.; Zhou, Y. All-Solid-State Flexible Microsupercapacitors Based on Reduced Graphene Oxide/Multi-Walled Carbon Nanotube Composite Electrodes. *Appl. Surf. Sci.* **2018**, *435*, 1228-1236.
49. Wang, D.; Fang, G.; Zheng, Q.; Geng, G.; Ma, J. Construction of Hierarchical Porous

Graphene–Carbon Nanotubes Hybrid with High Surface Area for High Performance Supercapacitor Applications. *J. Solid State Electr.* **2017**, *21*, 563-571.

50. Krishnamoorthy, K.; Pazhamalaia, P.; Kima, S.-J. Ruthenium Sulfide Nanoparticles as a New Pseudocapacitive Material for Supercapacitor. *Electrochim. Acta* **2017**, *227*, 85-94.

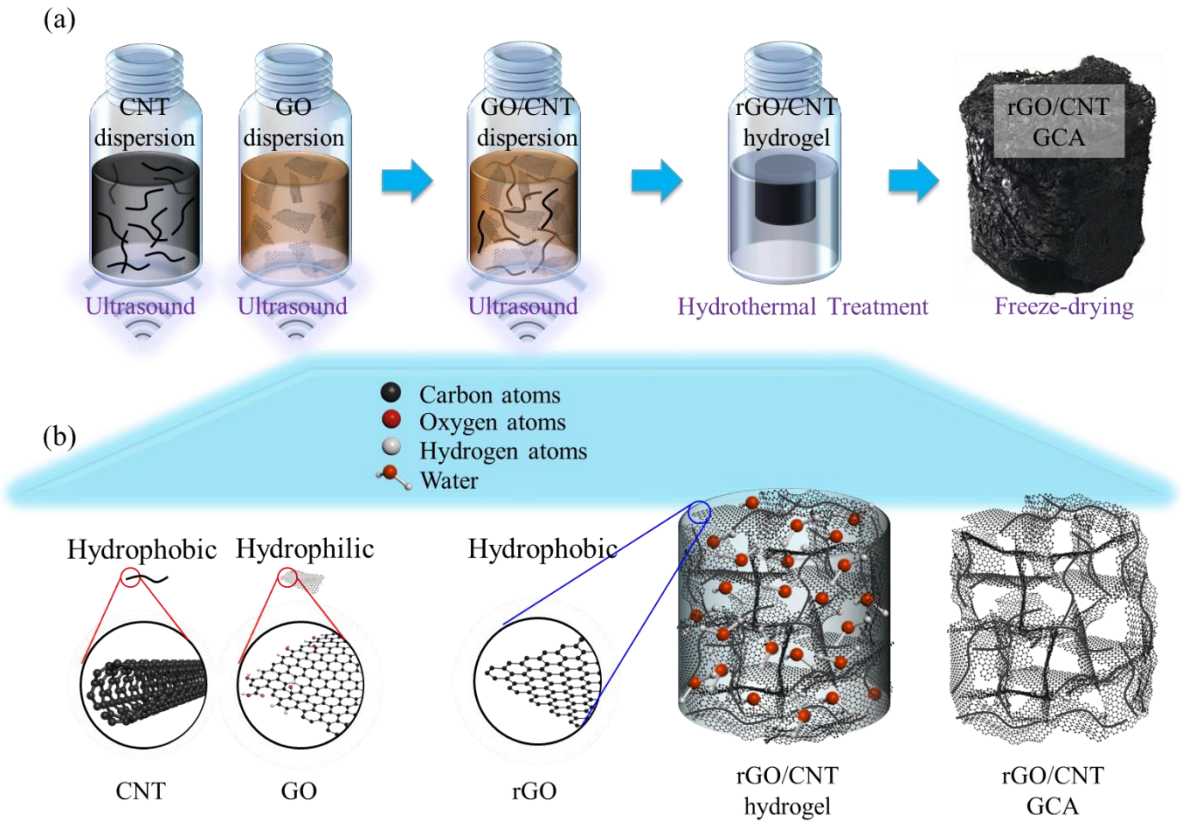

Figure 1. (a) Schematics illustration of the fabrication process of GCA. (b) An atomistic illustration of the microstructure of CNT, GO, rGO, rGO/CNT hydrogel, and GCA.

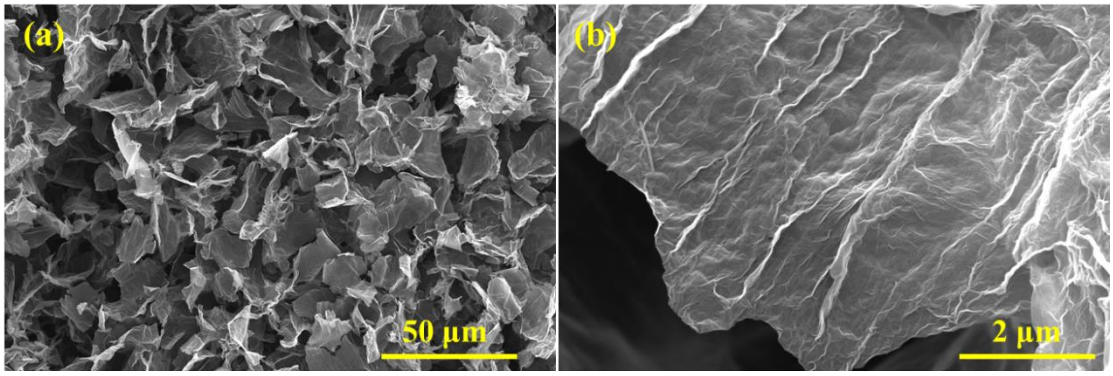

Figure 2. SEM images of GA at different magnifications.

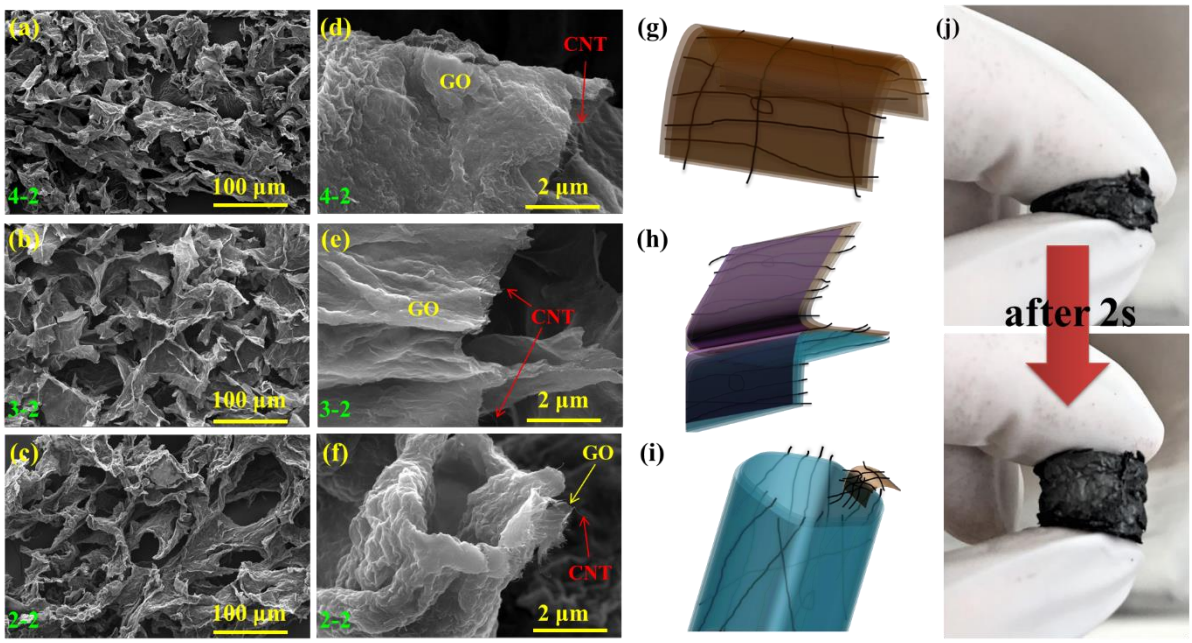

Figure 3. (a-c) SEM images of GCA 4-2, GCA 3-2, and GCA 2-2. (d-f) SEM images of different interconnections based on the CNT contents: (d) GCA 4-2, (e) GCA 3-2, and (f) GCA 2-2. (g-i) Cross-section models correspond to the three interconnection styles shown in (d-f), respectively. (j) Snapshot image of GCA 2-2 with excellent elasticity.

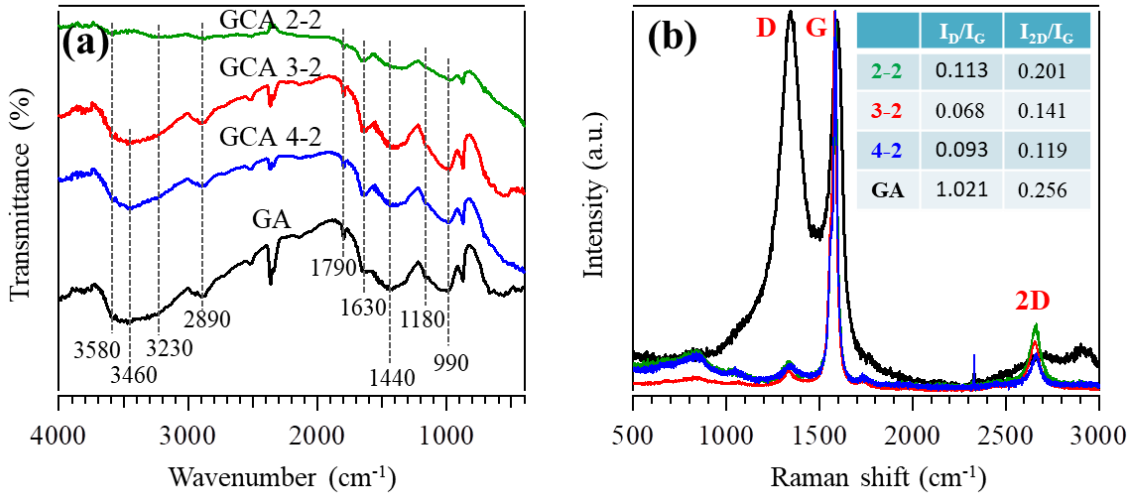

	I_D/I_G	I_{2D}/I_G
2-2	0.113	0.201
3-2	0.068	0.141
4-2	0.093	0.119
GA	1.021	0.256

Figure 4. (a) FTIR spectra. (b) Raman spectra of GA, GCA4-2, GCA3-2, and GCA2-2.

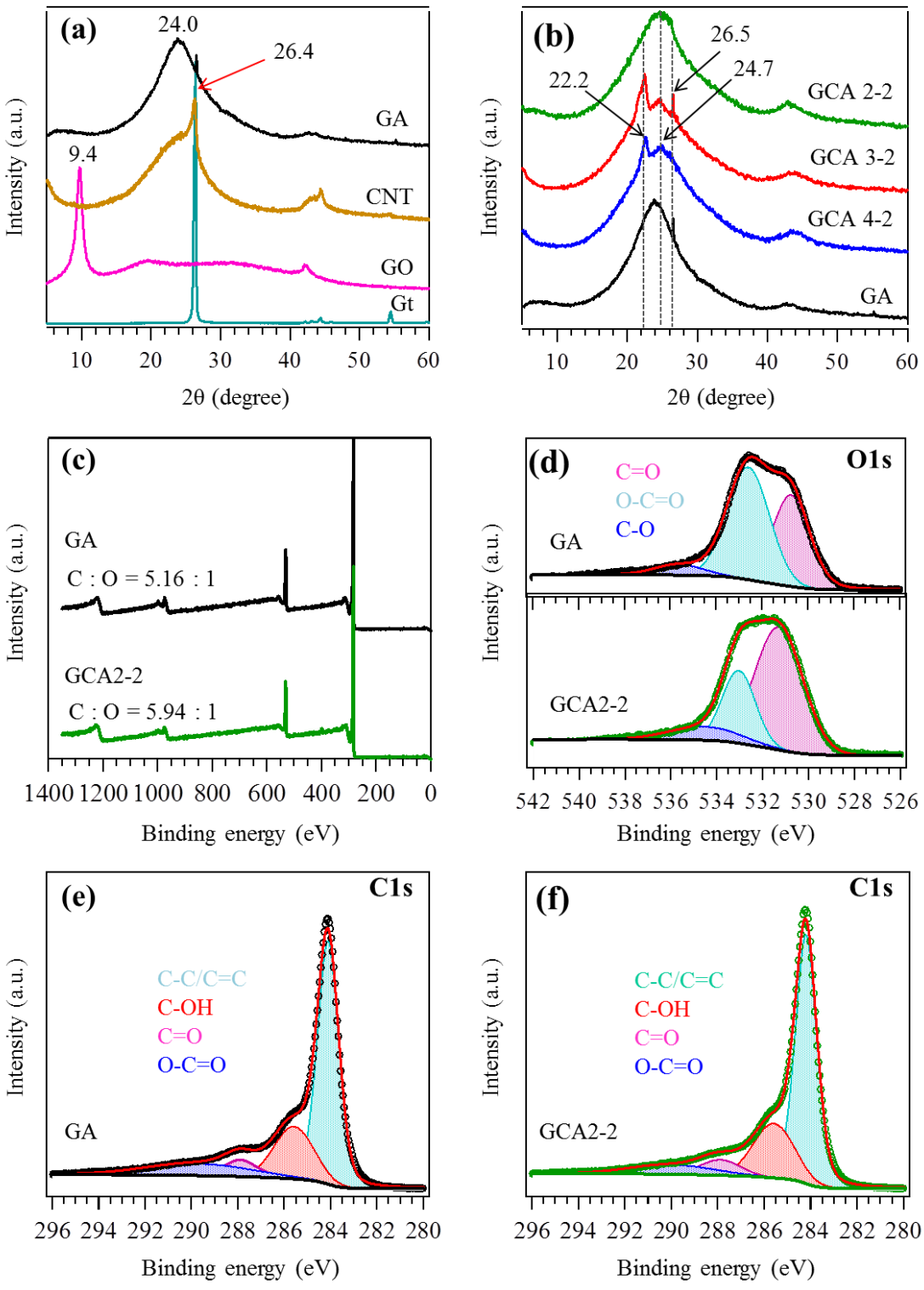

Figure 5. (a, b) XRD patterns, (c~f) XPS spectra of GA and GCA2-2.

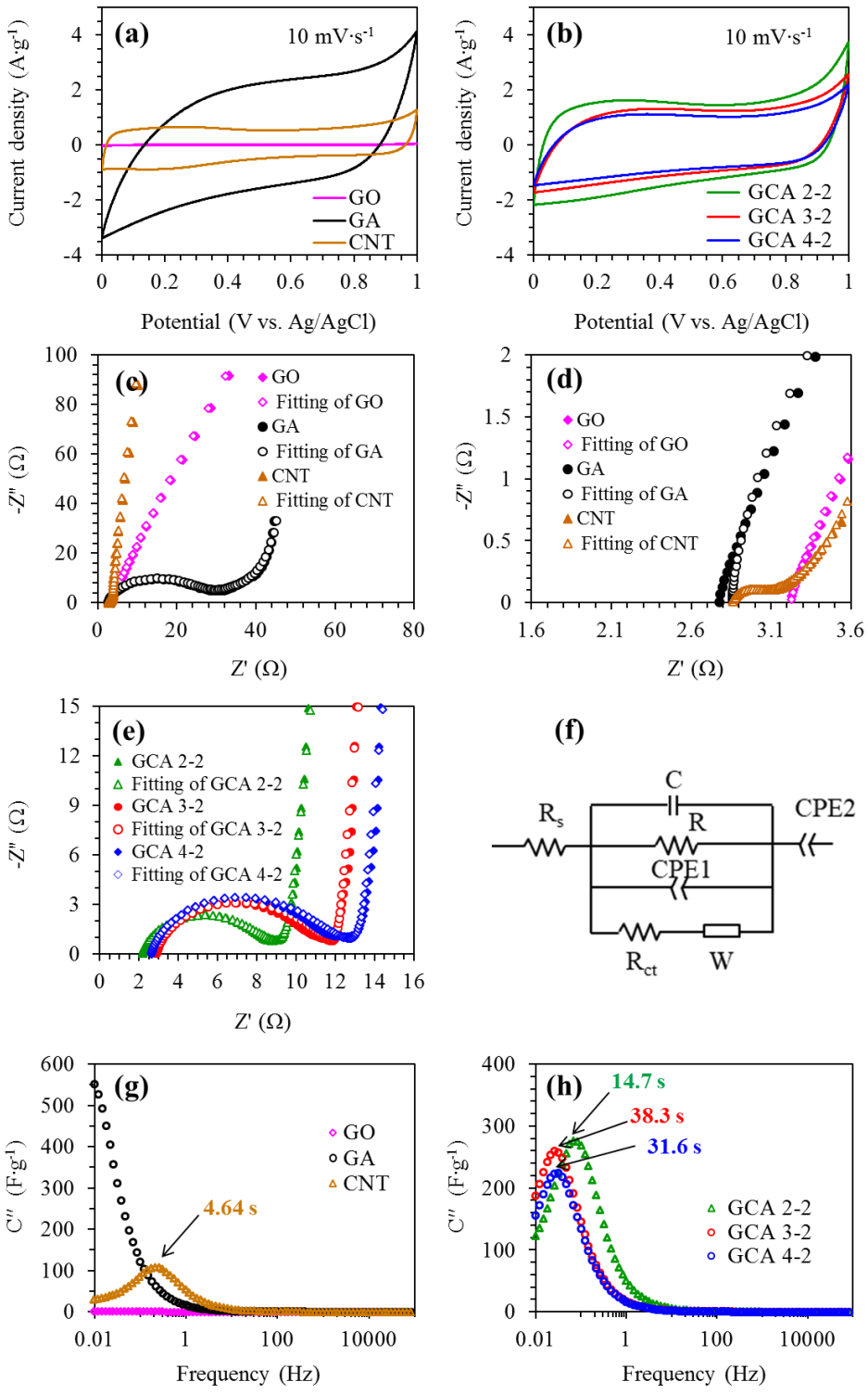

Figure 6. Electrochemical charge and ion transfer and storage performance in hybridised GO and CNT aerogels. (a, b) CV curves at a scan rate of 10 $mV \cdot s^{-1}$, (c, d, e) Nyquist plot, (f) equivalent circuits, Bode plots of (g, h) imaginary capacitance C″ *vs* Frequency.

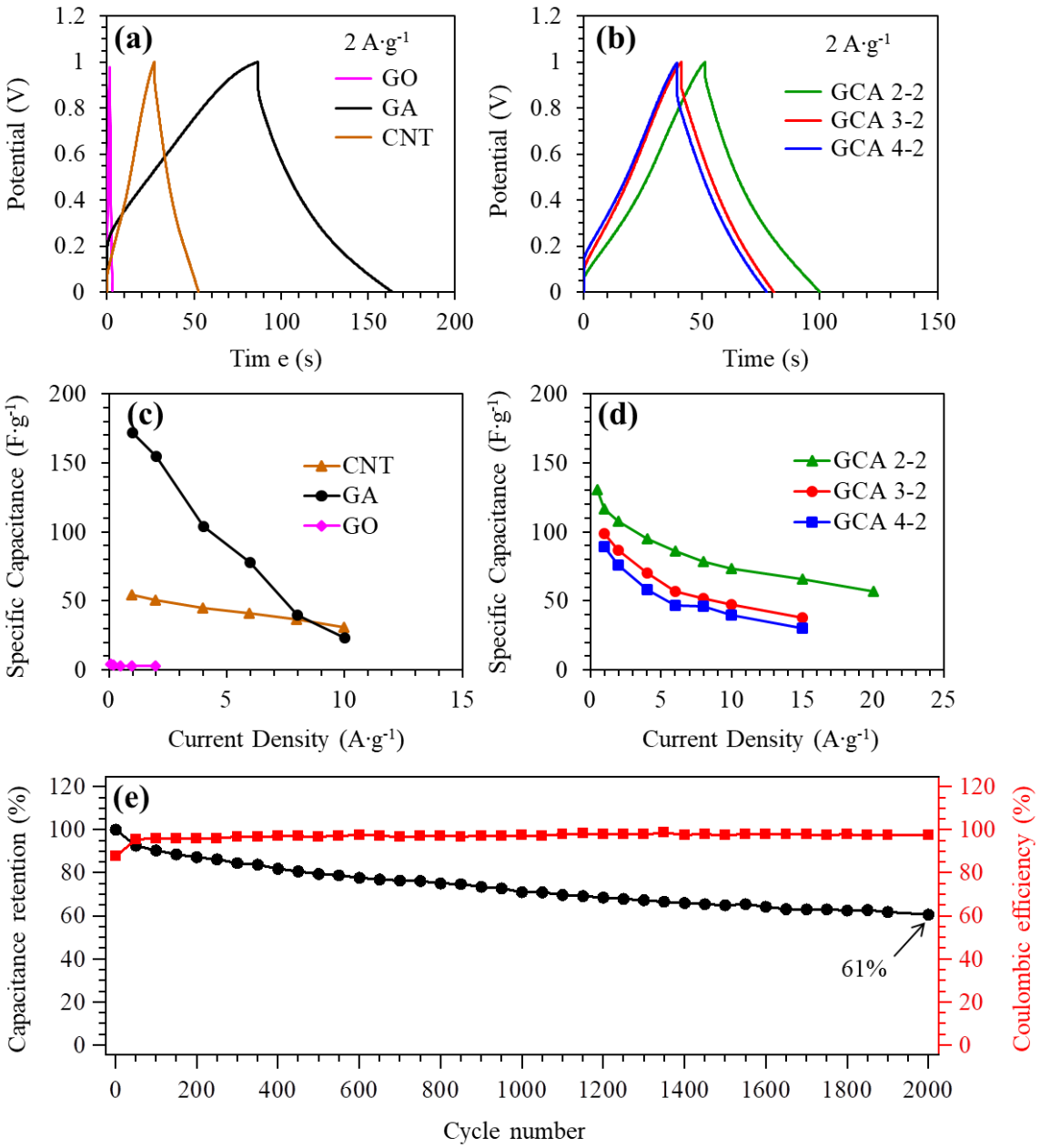

Figure 7. Rationalised supercapacitor performance of GO, GA, CNT and hybridised GCA aerogels. (a, b) GCD curves at a current density of 2 $A \cdot g^{-1}$. (c, d) specific capacitance *vs* the current density. (e) Cycling stability of GCA 2-2 based supercapacitor over 2000 cycles at a current density of 2 $A \cdot g^{-1}$.

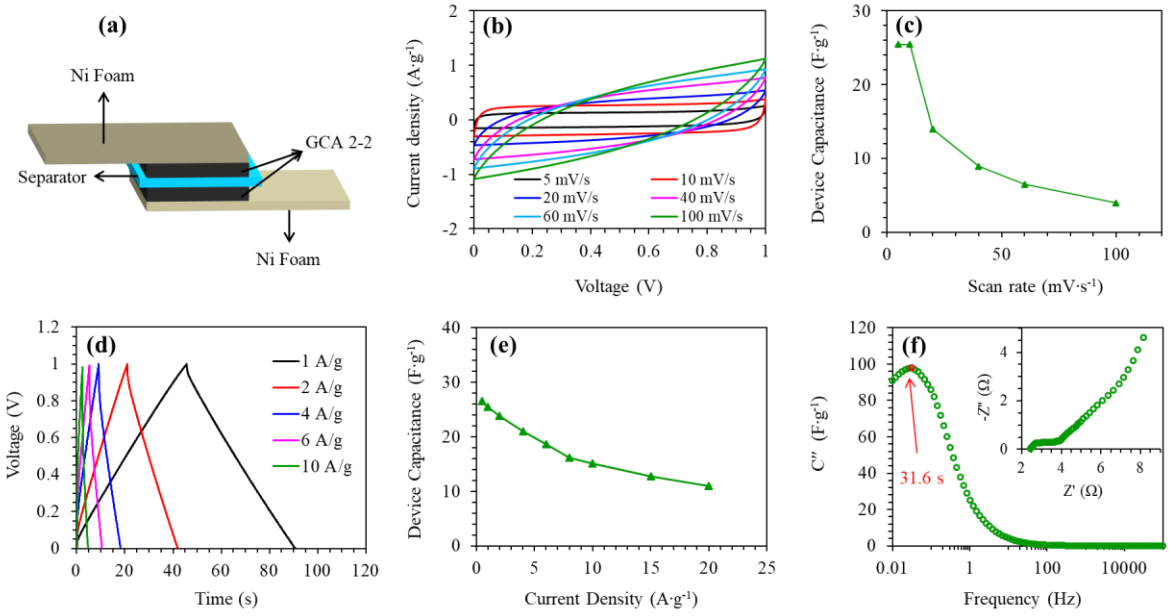

Figure 8. (a) Schematic illustration of the as-prepared symmetrical supercapacitor configuration. (b) CV curves at different scan rates. (c) The effects of the scan rate on the specific capacitance. (d) GCD curves at different current densities. (e) Specific capacitance *vs* the current density. (f) imaginary capacitance C″ *vs* Frequency and Nyquist plot (inset).

TOC Graphic

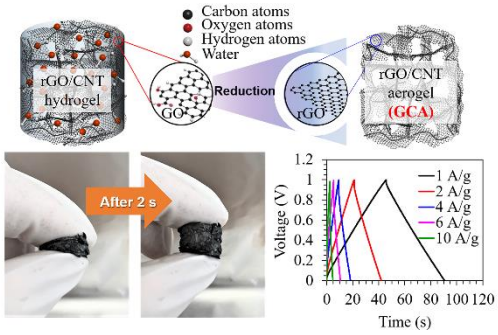
Carbon atoms
Oxygen atoms
Hydrogen atoms
Water
rGO/CNT
hydrogel
GO
Reduction
rGO
rGO/CNT
aerogel
(GCA)
After 2 s
Voltage (V)
Time (s)
1 A/g
2 A/g
4 A/g
6 A/g
10 A/g